Proceeding *20th SEAGC - 3rd AGSSEA Conference in conjunction with 22nd Annual Indonesian National Conference on Geotechnical Engineering.* Jakarta - INDONESIA, 6 -7 November 2018. ISBN No. 978-602-17221-6-9

A Case Study on Monitoring and Numerical Analysis of Groundwater Variation and Inclinometer Displacement in Taiwan

Ching-Jiang Jeng [1] and Chia-Yu Yang [1]
[1] *Department Environmental and Hazards-resistant Design, Huafan University, New Taipei City, Taiwan*
E-mail: jcjhf@cc.hfu.edu.tw

ABSTRACT: This study examined monitoring and numerical analysis results of a dip slope case in New Taipei City, Taiwan. The displacement data collected over the years by the inclinometers are used to study the creep of the slope, and combined with the influence of the typhoon rainfall. The time lag and groundwater level changes and the effectiveness of the implementation of two catchpits in the slope are reviewed. The Shape Acceleration Array (SAA) measurement is taken as the reference basis for hazard prevention and maintenance of the slope. Geostudio is applied to analyze the relationship between rainfall infiltration, groundwater level, and the displacement of the entire slope.
Keywords: Groundwater variation, inclinometer, SAA, numerical analysis.

1. INTRODUCTION

This study deal with the data obtained from monitoring system of dip slope area at the Huafan University in northeastern Taiwan as shown in Figure 1.

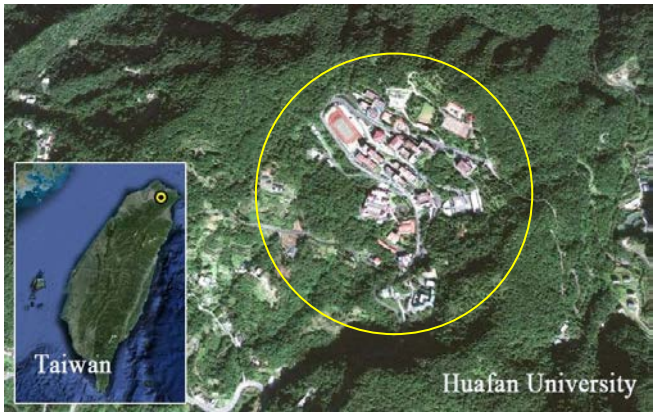

Figure 1 Location of the study site

Jeng and Sue (2016) analyzed the monitoring data collected from more than 300 settlement and displacement observation marks on this site and compared them with the displacement recorded by the inclinometers, concluding that a rise in the groundwater table caused by typhoons is the most critical factor in slope stability. Therefore, several countermeasures, including catchpits with horizontal drainage pipes, were recommended. The Japan Association for Slope Disaster Management (JASDiM) recommended the threshold values of slope displacement for different sliding stages, which were used to define three ranges. Generally, slope displacement can be distinguished into several stages, in which the three stages are: "initial displacement," "constant velocity displacement," and "accelerated increment displacement." Xu (2011) pointed out obvious stages characteristics for the gradual evolution of slope variations. To classify a type of displacement into one of the three stages, the s-t curve for the relationship between displacement and time can be converted into a T-t curve. The curve after conversion has a unique and deterministic tangent angle (α). Normally, the tangent angle of the curve is greater than 45 degrees when it enters the acceleration stage.

2. MONITORING SYSTEM AND SITE INFORMATION

The monitoring system set up in this site includes inclinometers, tiltmeters, crack gages, water-level observation wells, settlement and displacement monitoring marks, rebar strain gages, concrete strain gages, and rain gages. All of these monitoring instruments Figure 2 are continuously operational in taking regular measurements (see Jeng and Lin, 2011; Jeng and Jiang, 2013; Jeng et al., 2015, 2017).

The main exposed stratum under the site is the Mushan Formation, with the bedrock being mainly interbedded with sandstone and shale. It is a dip slope striking toward the east, dipping southward about 10°–20°. Huang and Jeng (2004) pointed out that through the observation and comparison of drilling cores and ground resistance images, as well as topographical characteristics, there are two local small faults: a south-trending Nanshihkeng Fault and a northwest-trending A Fault, as shown in Figure 3.

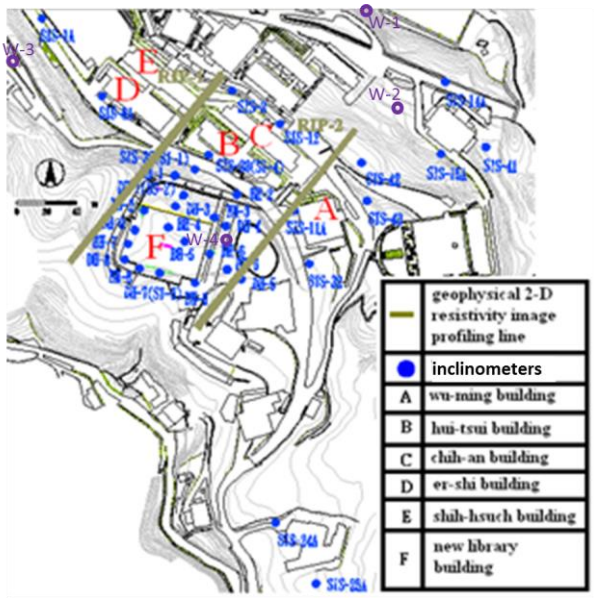

Figure 2 Inclinometer distribution and 2-D resisstivity image profiles line

3. ANALYSIS OF MONITORING RESULTS

3.1 Groundwater Variation Caused by Rainfall

Four sets of auto-recording groundwater-level gauges are designed in this research area for observation as shown in Figure 2. Additionally, Figure 4 illustrates one of the monthly rainfall data and groundwater-level changes in 2016. The rainfall types can be classified as post-peak rainfall, pre-peak rainfall, and pre-peak rainfall, respectively. Additionally, when rainfall occurs, groundwater level also changes, although with some time lag. The degree of groundwater level change is W1>W2>W3>W4, which indicates that degree of change of the groundwater level in observation wells is different across different regions. The W1 groundwater level change is particularly evident, with the groundwater level change uplifted by rainfall up to about 23 m, while in W2, W3, and W4, the amount of change was about 8 m, 6 m, and 1 m, respectively. This indicates that the groundwater level in the area of W1 was more susceptible to rainfall influence. A

comparison of different rainfalls shows that the peak rainfall of post-peak rainfall was greater than the peak of other types of rainfall. During the typhoon season, rainfall will cause greater rise of the groundwater level, and the lag time between the peak rainfall and peak groundwater level will significantly shorten. When the groundwater level in W1 rises to about ground level (GL) -30 m, W2 and W3 will then increase more noticeably.

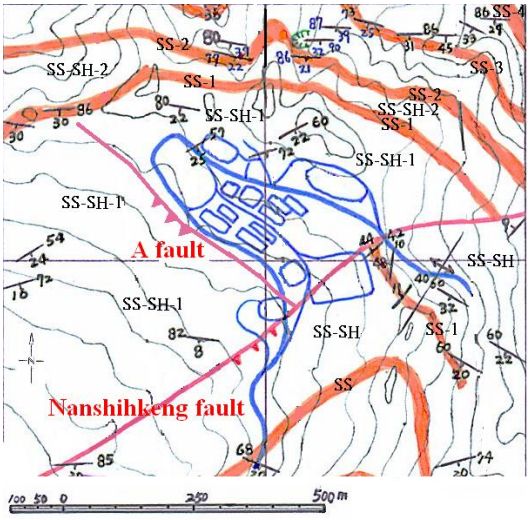

Figure 3 Site geological map

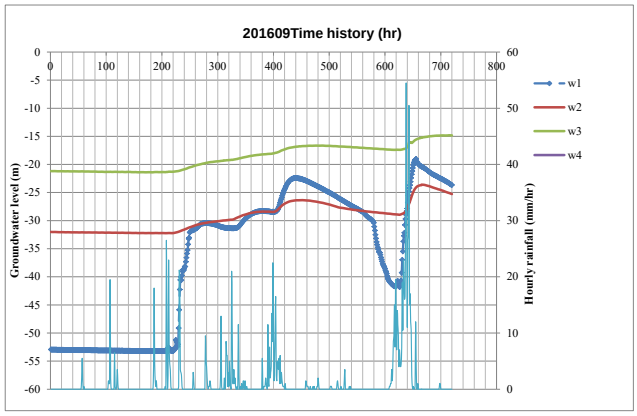

Figure 4 Groundwater level and rainfall duration curves in September 2016.

Groundwater-level change caused by rainfall can vary due to (1) rainfall type, (2) rainfall amount, (3) rainfall time lag, (4) groundwater-level gauge region, and (5) seasonal factors. Analyses of these factors are illustrated in Figs. 5–7, which contain only analysis data from observation well W1. These figures are, in this order, the groundwater level and rainfall peak time lag diagram, the peak rainfall and groundwater-level rise diagram, and the accumulated rainfall and groundwater-level rise diagram for W1 groundwater-level gauge from 2013 to 2015. Figure 5 is the groundwater level and rainfall peak time lag diagram of automatic groundwater-level gauge W1. The x-axis is the peak rainfall, and the y-axis is the time lag for groundwater level to reach its peak. Figure 6 is the peak rainfall and groundwater level rise diagram of automatic groundwater-level gauge W1. The x-axis is the peak rainfall, and the y-axis is the amount of groundwater level rise. Figure 7 is the accumulated rainfall and groundwater-level rise diagram of automatic groundwater-level gauge W1. The x-axis is the accumulated rainfall, and the y-axis is the groundwater-level rise amount. The round dots are post-peak rainfalls, the square dots are pre-peak rainfalls, and the triangle dots are middle-peak rainfalls. There are two types of accumulated rainfall: accumulated up to the peak (dark-colored symbols) and accumulated for the entire rainfall (light-colored symbols).

Figure 5 shows that the greater the peak rainfall, the shorter the reaction time lag is for the groundwater level to rise. With respect to the rainfall type perspective, the peak rainfall of the pre-peak rainfalls is concentrated less than 20 mm and has a long groundwater-level time lag. The peak rainfall of the middle-peak rainfalls ranges from 20 mm to 40 mm, and the peak rainfall of the post-peak rainfalls is concentrated at around 50 mm with a short time lag. It indicates that if this study area has rainfall greater than 50 mm, it should be closely observed and the observation time should be stretched to about 40 hours. Further, Figure 6 shows that for greater peak rainfall, the groundwater level will significantly increase, and the post-peak rainfall will cause the most significant groundwater level rise. According to the auto-recording groundwater-level gauge, the groundwater rise amount was between 1 and 23 m. Lastly, Figure 7 shows that when the total average cumulative rainfall to peak point exceeds 200 mm, the groundwater level in auto-recording groundwater-level gauge in W1 will increase up to 20–23 m.

As mentioned above, when the peak rainfall is greater, the time lag of the groundwater level rise will be shorter. The peak rainfall of the post-peak rainfall type is greater than that of other rainfall types, which makes the change of its groundwater level significant. Thus, observation for up to 40 hours is needed for the post-peak rainfall. The data from the auto-recording groundwater-level gauge shows that the groundwater level W1 is most affected by rainfall, with a change between 1 m and 23 m. A groundwater-level change of 0.6–5.8 m was found in the auto-recording groundwater-level gauge in W2, 0.25–3.1 m in W3, and 0.1–2 m in W4.

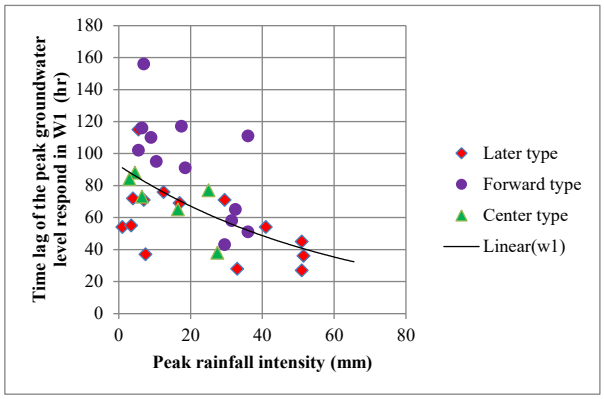

Figure 5 Groundwater level and time lag of rainfall peak diagram of automatic groundwater-level gauge W1.

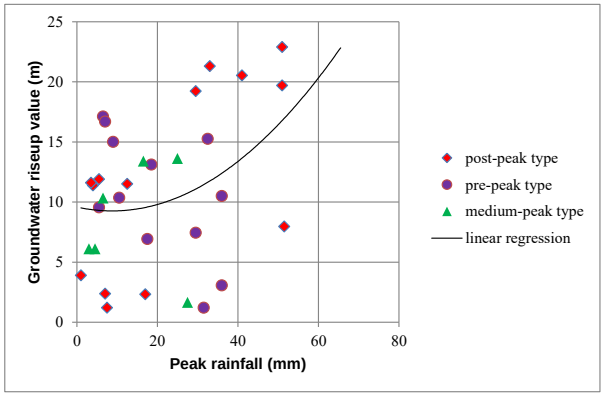

Figure 6 Peak rainfall and groundwater level rise diagram of automatic groundwater-level gauge W1.

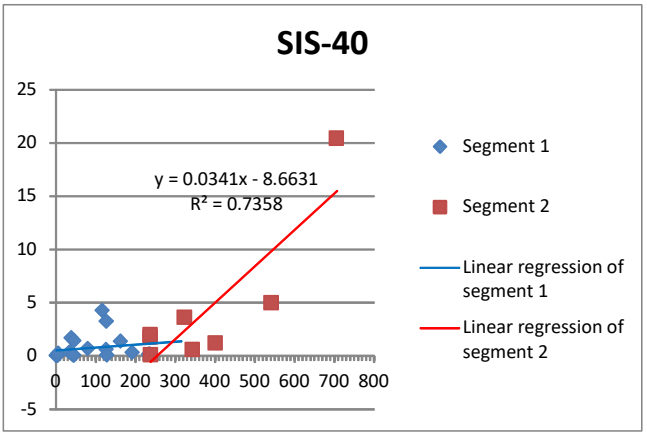

Figure 7 Accumulated rainfall and groundwater level rise diagram of automatic groundwater-level gauge W1.

3.2 Inclinometer Displacement Triggered by Typhoons

Figure 8 is the SIS-40 displacement and cumulative rainfall amount from typhoon rainfall. The x-axis is the cumulative rainfall amount from typhoon rainfall, and the y-axis is the displacement caused. Different inclinometer displacements from different typhoons in the past years are presented in the graph. Once the displacement starts to accelerate, the accumulated rainfall is treated as an alert rainfall threshold value. Figure 12 shows the typhoon cumulative rainfall alert of SIS-40 has a threshold of about 350 mm. The typhoon cumulative rainfall alert threshold values from the other nine inclinometers are summarized and shows that the alert cumulative rainfall threshold for heavy typhoon rainfall causing campus slope displacement is approximately 315–495 mm.

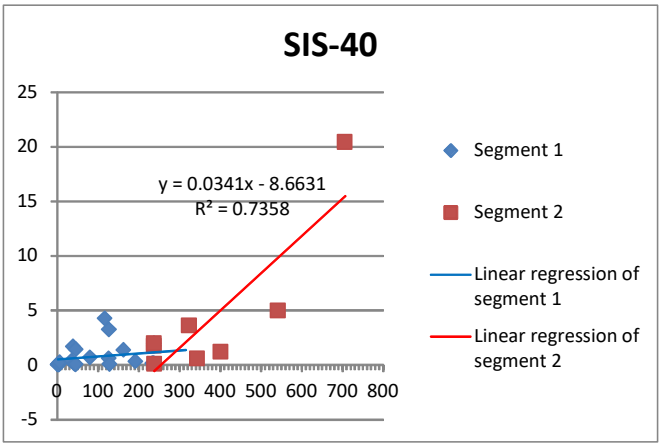

Figure 8 SIS-40 displacement and cumulative rainfall amount from typhoon rainfall.

3.3 Comparison of Groundwater Level Change to Explore the Effectiveness of Catchpits

Figure 9 is the relation graph of rainfall data and groundwater level from the auto-recording groundwater-level gauge from April to July 2016. The x-axis is time, the left y-axis is the water level, and the right y-axis is the rainfall amount of the day. The groundwater level from the auto-recording groundwater-level gauge in W1 has a red curve, the water level in W2 has a green curve, the water level in W3 has a purple curve, and the groundwater level in W4 has a light blue curve. The dark-blue curve shows the daily rainfall amount from April to July. The figure shows that, similar to aforementioned data, W1 is much more affected by the rainfall amount than the other three auto-recording groundwater-level gauges. The data from the auto-recording groundwater-level gauge in W1 from 2013 to 2016, as shown in Figure 10, shows that the normal groundwater level from the auto-recording groundwater-level gauge in W1 has a lowest value of about −43.67 m from 2013 to 2015. After the implementation of the catchpits in 2016, the lowest curve has decreased significantly to −52.03 m. The highest groundwater level also dropped from −22.67 m to −27.84 m. This is due to the implementation of the two catchpits at the site, which significantly reduced both normal groundwater level and the highest groundwater level during rainy and typhoon seasons.

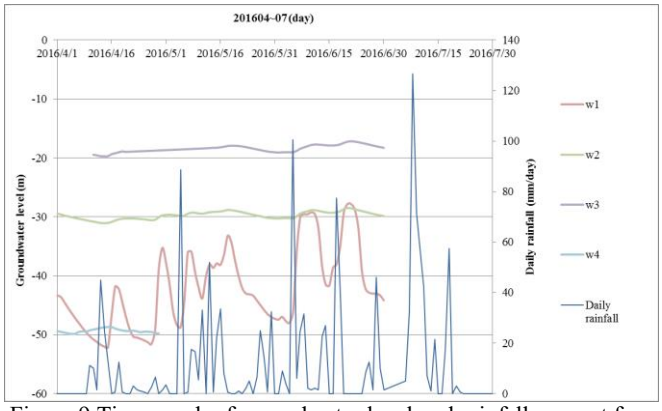

Figure 9 Time graph of groundwater level and rainfall amount from auto-recording groundwater-level gauge from April to July 2016.

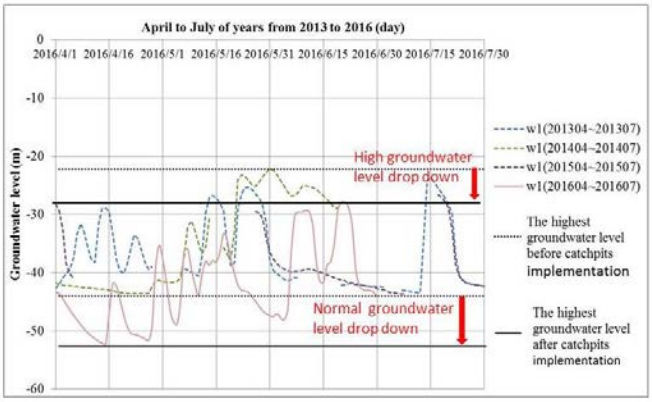

Figure 10 Comparison of groundwater level before and after catchpits implementation.

3.4 Discussion of SAA displacement measurement results

This study sought to understand slope displacement caused by typhoon rainfall, so the collection of rainfall data and SAA displacement data continued until February 2017 to observe and analyze the relationship between typhoon rainfall and displacement of SAA. In this paper, only part of the data was taken and enlarged, shown in Figs. 11–12. The x-axis is the date, the left y-axis is the rainfall amount, and the right y-axis shows the accumulated displacement of inclinometer SIS-11 and inclinometer SIS-20.

As shown Figures 11 to 12, there were two typhoons in August 2015, the medium typhoon Soudelor and the strong typhoon Goni. Accordingly, SIS-11 had displacement of 6.048 mm and 1.489 mm, respectively, and the displacement of SIS-20 was 4.839 mm and 1.64 mm, respectively. In October 2016, there was light typhoon Aere along with its peripheral circulation. SIS-11 had a consequent displacement of 11.321 mm, while SIS-20 had a displacement of 3.384 mm. The above data are plotted in Figure 13 as an SAA displacement increment graph during typhoon rainfall.

Figure 13 shows that when the typhoon cumulative rainfall reaches 184 mm, significant displacement will occur; when the cumulative rainfall reaches 300 mm or more, or when the peak rainfall exceeds 156 mm, the displacement will begin to accelerate, producing displacement larger than 3 mm. This result agrees with that in Section 3.2 of this study. Therefore, the study sets typhoon rainfall of more than 300 mm as the alert threshold. In other words,

if the weather forecast reports a typhoon rainfall of more than 300 mm, then the displacement situation should be closely monitored.

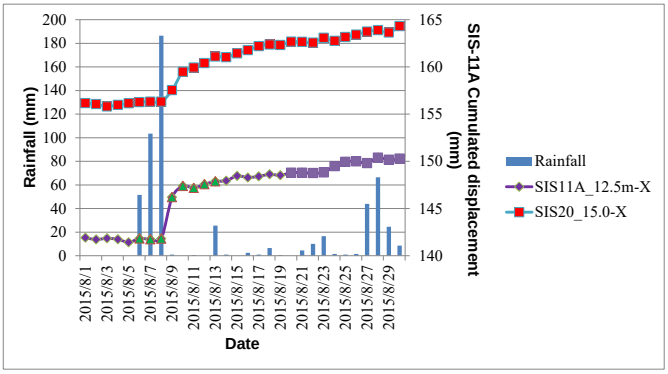

Figure 11 SIS-11 and SIS-20 displacement versus rainfall amount in August 2015.

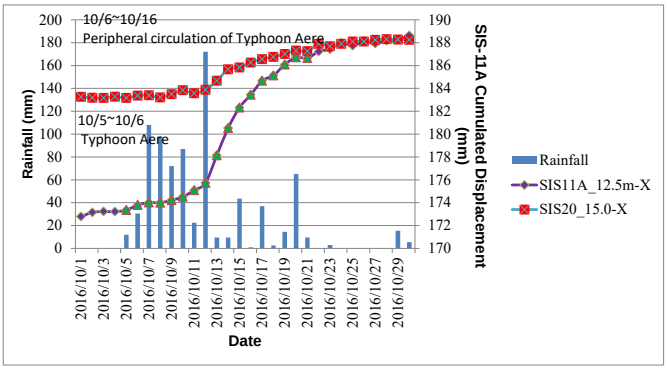

Figure 12 SIS-11 and SIS-20 displacement versus rainfall amount in October 2016.

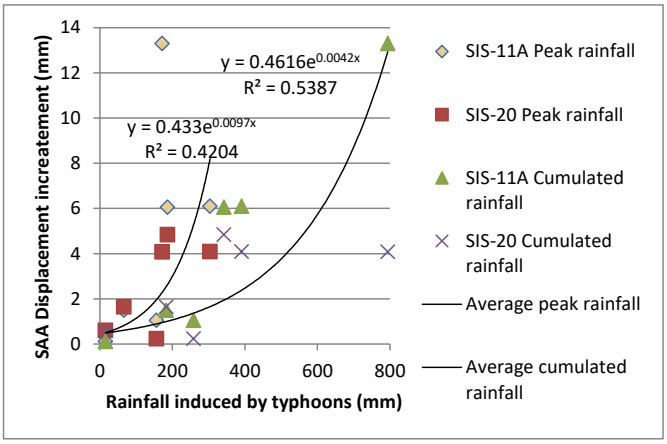

Figure 13 SAA displacement increment during typhoon rainfall.

4. NUMERICAL ANALYSIS OF GEOSTUDIO SIMULATION

In this study, the geological and hydrological data of the site were entered into GeoStudio software to carry out SEEP/W, SLOPE/W, and SIGMA/W numerical analysis. The simulation results were compared to the monitoring data to analyze the effect of rainfall on the slope. The initial condition setting: boundary conditions of rainfall infiltration are shown in Figure 14, wherein AB is a boundary of the lower constant head slope, and the total head height is set to H = 387.8 m; CD is the head boundary of the upper slope, and the total head height is set to H = 534.5 m. The upper and lower boundaries of the head setting mainly use the average groundwater level from historical monitoring data. The BC is the impervious boundary (Q = 0); AD is the boundary of rainfall infiltration. Table 1 shows the input parameter for the analysis

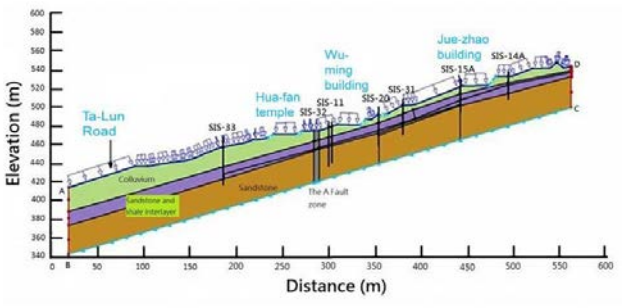

Figure 14 Cross-section profile of SEEP/W.

Table 1 Input Parameters for numerical analysis

Soil layer	Colluvium soil layer	Sandstone and shale interbedded	Gravel layer	Shear zone
Deformation model	Elastoplastic	Elastoplastic	Linear elasticity	Interface elements
Elastic modulus (kPa)	3×10^4	3.225×10^5	3.753×10^6	3748
Poisson's ratio	0.334	0.28	0.23	0.334
Unit weight (kN/ m^2)	19.31	25.52	23.86	23.3
Cohesion, C (kN/ m^2)	18.5	41.8	38.7	0
Internal friction angle, Φ (degrees)	29.6	32.13	32.74	23

This study used rainfall data during typhoons in August 2015 and October 2016, the amount of groundwater-level variations from four auto-recording water-level gauges, as well as two auto-recording inclinometer SAAs, to observe and analyze the relationship between rainfall amount during typhoon, slope displacement, and groundwater-level variation. The results are aggregated to show the trend. Two typhoons struck in August 2015, the typhoon Soudelor during 8/6–8/9, and the typhoon Goni during 8/20–8/23. Soudelor generated a rainfall amount of 342.5 mm, an SIS-11A displacement increment of 6.048 mm, and an SIS-20A displacement increment of 4.893 mm. Typhoon Goni generated a rainfall amount of 30.5 mm, an SIS-11A displacement increment of 1.489 mm, and an SIS-20A displacement increment of 1.64 mm. A southern low-pressure system (typhoon Aere) generated a rainfall amount of 794 mm, an SIS-11A displacement increment of 11.321 mm, and an SIS-20A displacement increment of 3.384 mm. The rainfall amount and actual displacement data were used as a reference in the GeoStudio software simulation analysis. Figure 15 shows the case of SIS-20 and SIS-11 inclinometer displacement increment diagram during one of the typhoon Soudelor. These figures demonstrate the displacement result simulated by this model has the same displacement curve trend as the actual monitoring data.

This study adopted the Morgenstern-Price extreme balance method to calculate the safety factor of the sliding surface. Figure 16 shows the profile of SLOPE/W analysis. The most critical potential sliding surface existed between Jue-zhao building and Wu-ming building is shown in the profile. The results of safety factor variation during typhoon are shown in Figure 17. Figure 17 shows that during the Typhoons Aere , although the safety factor of the slope will drop to about 0.6, the minimum safety factor for rainfall can still be maintained at 1.2. This illustrates that even though typhoon rainfall will cause a certain amount of slope displacement at the campus, its safety factor is still higher than the general suggested value of 1.2; in other words, there is not yet immediate danger of sliding. However, further studies should investigate the impact on safety factors in situations of higher typhoon rainfall through actual follow-up test results and feedback analyses.

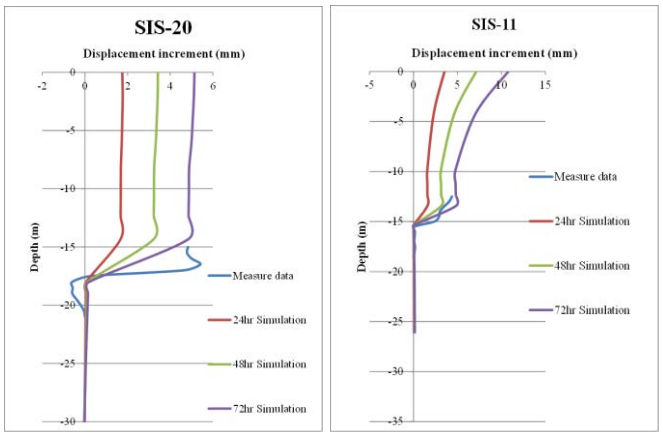

Figure 15 SIS-20 displacement increment (left) SIS-11 displacement increment (right) of simulation of the typhoon Soudelor.

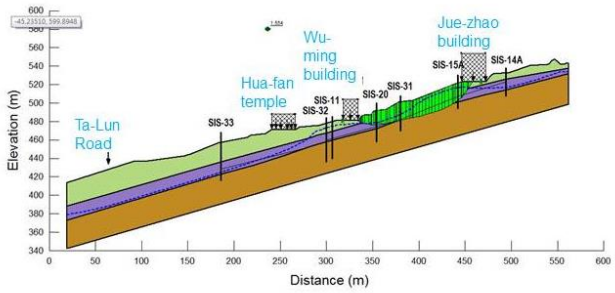

Figure 16 Profile of potential sliding surface analysis

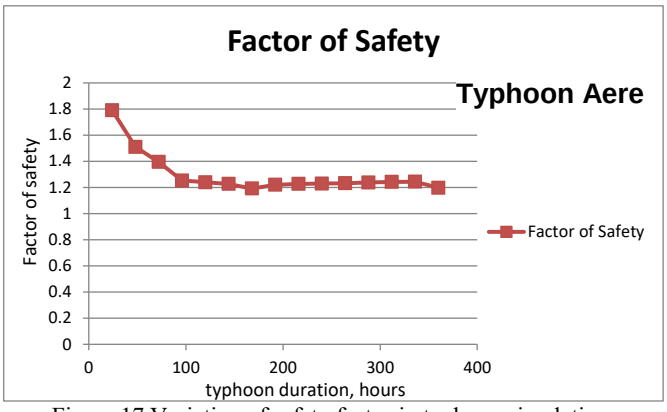

Figure 17 Variation of safety factor in typhoon simulation.

5. CONCLUSION

Based on the results, the following conclusions can be made:

1. The groundwater-level W1 is most affected by the rainfall, with a variation of 1–23 m. The groundwater level variation was 0.6–5.8 m for W2, 0.25–3.1 m for W3, and 0.1–2 m for W4. When the peak rainfall is higher, there is less delay of groundwater level rise, and the peak rainfall of post-peak rainfall is larger than that of other rain types, which makes the groundwater-level variation large. Thus, observation up to 40 hours is needed for post-peak rainfall type.
2. After the implementation of the catchpits, the lowest groundwater level has decreased from −43.67 m in 2015 to −52.03 m in 2016. The highest groundwater level also dropped from −22.67 m to −27.84 m. Therefore, the normal groundwater level and highest groundwater level has been significantly decreased during the rainy seasons and typhoon seasons by the draining effectiveness of the two catchpits.
3. When the typhoon cumulative rainfall reaches 184 mm, significant displacement will occur; when the cumulative rainfall reaches 300 mm or more, or when the peak hourly rainfall exceeds 100 mm, the displacement will begin to accelerate, producing displacement of larger than 3 mm. Therefore, the study sets typhoon rainfall of more than 300 mm as the alert threshold.
4. The typhoon Soudelor simulation shows that the displacement result simulated by this model has the same displacement curve trend as the actual monitoring data.
5. The result agrees with the results mentioned above; generally, only when the rainfall exceeds 77 mm will the displacement be driven. In other words, simulation results from the software using cumulative rainfall and peak rainfall greater than 60 mm will be more important and more meaningful than simulation results from simulating a single peak rainfall.
6. The slope model analytical results show that during the Typhoons Aere, although the safety factor of the slope will drop to 0.6, the minimum safety factor for rainfall was still maintained at 1.2, higher than the general suggested value of 1.2. This means that there is not yet any immediate danger of sliding.

6. REFERENCES

Huang, C. S. and Jeng, C. J.: A supplementary geological survey and analysis of the Talun area around the Huafan University. Journal of Art and Design of Huafan University, (1), 59–69, 2004.

Japan Landslide Association for Slope Disaster Management (JASDiM): Essential implementation of technical design for landslide countermeasures, (2), 22, 1978 (in Japanese).

Jeng C. J., and Lin, T. A.: A case study on the in-situ matrix suction monitoring and undisturbed-sample laboratory test for the unsaturated colluvium slope. Soils and Foundations, 51, (2), 321–331, 2011.

Jeng, C. J. and Jiang, J. R.: Research on serial behaviors of colluviums slope from rainfall infiltration caused ground water variation to the slope stability and displacements. Journal of Art and Design of Huafan University, (8), 17–31, 2013.

Jeng, C. J. and Yang, C. Y.: A case study on groundwater variation and slop displacement induced by rainfall. Journal of Art and Design of Huafan University, (10), 141–156, 2015.

Jeng, C. J. and Sue, D. Z.: Characteristics of ground motion and threshold values for colluvium slope displacement induced by heavy rainfall. Nat. Hazards Earth Syst. Sci., (16), 1309–1321, 2016.

Xu Q.: Early warning and emergency disposal of landslide disaster, state key laboratory of geohazard prevention and geoenvironment protection: An academic report in National Chung Hsing University, Taiwan, 2011.